metals

MDPI

Article

Metallurgical Properties of Lump Ore and Practice of High-Proportion Lump Ore for Low-Carbon Smelting of Blast Furnace

Yufeng Guo [1], Yanqin Xie [1], Lei Fang [2], Heming Ju [2], Shuai Wang [1,*], Feng Chen [1] and Lingzhi Yang [1]

[1] School of Minerals Processing and Bioengineering, Central South University, Changsha 410083, China
[2] Nanjing Steel Group Co., Ltd., Nanjing 210035, China
* Correspondence: wang_shuai@csu.edu.cn

Abstract

The existing blast furnace burden structure in China is mainly dominated by high-alkalinity sinter and acid pellets, with a relatively small proportion of lump ore blended in. Against the backdrop of the "dual-carbon" goals, iron and steel plants are under enormous pressure to save energy and reduce carbon emissions. Lump ore is directly extracted from mines and belongs to zero-carbon-emission blast furnace burden. Therefore, adjusting and optimizing the blast furnace burden structure by partially replacing sinter and pellets with lump ore is an important approach for iron and steel plants to reduce carbon emissions. Based on the metallurgical properties and decrepitation index of different types of lump ore as well as the proportion of lump ore charged into the blast furnace, and with full consideration of the interaction of the comprehensive metallurgical properties of the blended burden charged into the furnace, the metallurgical properties of sinter are adjusted to ensure good comprehensive metallurgical properties of the blended burden. By adjusting the blast furnace operation to an appropriate regime, the proportion of comprehensive lump ore in the charged burden has been achieved to be $\geq$28%, and the blast furnace fuel ratio to be $\leq$515 kg per ton of iron.

Keywords: lump ore; blast furnace burden; high-proportion; low carbon

1. Introduction

The current structure of blast furnace feed in China predominantly consists of high-alkalinity sinters and acidic pellets, with a relatively small proportion of lump ore being utilized [1,2]. Traditional ironmaking theory posits that a "high sintered ratio" (comprising sintered ore and pellets) exerts a positive influence on the blast furnace smelting process. This high ratio facilitates indirect reduction in the upper part of the blast furnace, thereby reducing the fuel ratio. Additionally, it enhances the softening and melting characteristics of iron-containing feed in the lower part of the blast furnace, improving permeability and fluidity [3,4]. However, pellets, as one of the "sintered materials", are significantly more expensive than natural lump ore. Furthermore, the production processes for sinters and pellets are characterized by high energy consumption, environmental pollution, and substantial carbon emissions [5–7].

Lump ore, which is directly derived from mining, represents a zero-carbon-emission blast furnace burden. Utilizing lump ore to partially replace sinter and pellets for optimizing the blast furnace burden structure is an important strategy to achieve carbon emission

Check for updates

Academic Editor: Andrea Di Schino

Received: 22 October 2025
Revised: 12 December 2025
Accepted: 18 December 2025
Published: 22 December 2025

Copyright: © 2025 by the authors. Licensee MDPI, Basel, Switzerland. This article is an open access article distributed under the terms and conditions of the Creative Commons Attribution (CC BY) license.

reductions in ironmaking [8]. Clearly, from the perspectives of equipment investment, energy consumption, resource security, and environmental protection, it is advantageous for blast furnaces to employ a higher proportion of high-grade natural lump ore [9].

With the rapid advancement of the ironmaking industry in China, the technological level of blast furnace ironmaking has made significant progress, one manifestation of which is the increasing proportion of natural lump ore in the burden structure [10–18]. Numerous production practices have demonstrated that natural lump ore has both advantages and disadvantages in blast furnace smelting. The advantages include the following: some types of lump ore can enhance the furnace feed grade and reduce agglomeration costs; lump ore possesses a significant price advantage compared to pellets; natural lump ore does not generate pollutants during the iron ore powder agglomeration process; certain types of lump ore exhibit good indirect reducibility within the furnace, leading to a high utilization rate of furnace top gas, which is conducive to reducing the coke ratio. However, there are also some adverse effects associated with the use of lump ore [19–23]: lump ore can produce a substantial amount of powder after long-distance transportation, transfer, and friction; some lump ore is challenging to screen; the thermal bursting of lump ore in the furnace can generate a considerable amount of powder; certain types of lump ore are more compact and have slightly inferior reducibility; the softening and melting performance of a single type of lump ore is suboptimal, and excessive use can significantly impact the soft-melting and dripping performance of the lower part of the blast furnace. Therefore, it is crucial to investigate the performance of blast furnace smelting under a high proportion of lump ore to ensure the smooth operation of the blast furnace.

As shown in Table 1, several major steel companies in China have successfully increased their lump ore ratio through industrial trials, achieving favorable operational results.

Table 1. Some industrial practices to increase the proportion of lump ore in China.

Steel Company	Lump Ore Proportion/%	References
AnSteel	17.5	[15]
HanSteel	21.5	[24]
ShaoSteel	23	[11]
Xingcheng Steel	18–20	[25]
Delong Steel	17–20	[26]
Xinyu Steel	15.4	[17]

AnSteel's trials demonstrated that lump ore with a medium-to-high metallurgical value can serve as an effective auxiliary ironmaking material. Its use correlated with an increase in the blast furnace utilization coefficient and a decrease in the fuel ratio [15]. Similarly, ShaoSteel raised its lump ore proportion to substitute for more expensive pellets. This was achieved by enhancing raw material quality for process stability and closely monitoring key operational parameters, such as pressure differential and furnace thermal load. Through continuous optimization, ShaoSteel increased the lump ore proportion in the burden from 15% to over 23%, securing significant economic benefits [11]. HanSteel addressed the specific challenges of lump ore smelting by implementing measures including strategic selection of lump ore varieties, control of the slag's MgO/Al_2O_3 ratio, installation of lump ore drying equipment, and adjustments to the charging and blast systems. Consequently, the company achieved an average lump ore proportion of 21.5% [24].

Increasing the lump ore ratio is now recognized as a significant measure for energy conservation, emission reduction, environmental protection, and cost reduction [9,25–27]. However, a high lump ore ratio substantially influences burden distribution in the stack, the characteristics of the solid-state charge, and the properties of the softening–melting

zone. As blast furnace operation requires a stable slag system, any increase in lump ore usage must maintain this stability [28–30].

Therefore, this study systematically investigates the following under high-lump-ore conditions: (1) the evolution of lump ore in the solid-state zone, (2) its softening and dripping behavior in the cohesive zone, and (3) the optimization of the overall burden structure. The objective is to clarify the appropriate operational system for blast furnaces employing high lump ore burdens and to develop corresponding technologies for low-carbon and efficient smelting.

2. Materials and Methods

2.1. Materials

The raw materials for this study consisted of lump ore, sinter, and pellets; their chemical compositions are provided in Table 2. The low-silicon lump ore was commercially sourced from Nanjing steel plant (Nanjing, China). As indicated in the table, the lump ore exhibits the highest total iron (TFe) content. Its gangue is composed predominantly of SiO_2 (2.38%) and Al_2O_3 (1.58%). The loss on ignition (LOI) for the lump ore is 5.99%.

Table 2. Chemical compositions of raw materials (wt%).

Kinds	TFe	FeO	SiO_2	CaO	MgO	Al_2O_3	LOI
Lump ore	62.69	1.01	2.38	0.16	0.14	1.58	5.99
Pellets	62.27	0.30	6.29	1.80	0.77	1.62	/
Sinter	54.63	9.13	5.53	11.50	2.16	2.53	/

The appearance and morphology of the lump ore, sinter, and pellets are shown in Figure 1. The particle size distribution of the lump ore (Table 3) is primarily concentrated in the 16–25 mm range, with a significant proportion of coarser particles.



(**a**) lump ore (**b**) sinter (**c**) pellets

Figure 1. Appearance and morphology of different blast furnace feeds.

Table 3. Particle size distribution of lump ore (wt%).

−10 mm	10~16 mm	16~25 mm	25~40 mm
8.01	19.09	51.93	20.97

The phase composition of the lump ore is presented in Figure 2. The main crystalline phases identified are hematite (Fe_2O_3) and goethite (FeO(OH)), classifying the material as a limonite ore. Quantitative Rietveld refinement indicates an approximate 1:1 ratio, with each phase constituting roughly 50% of the sample.

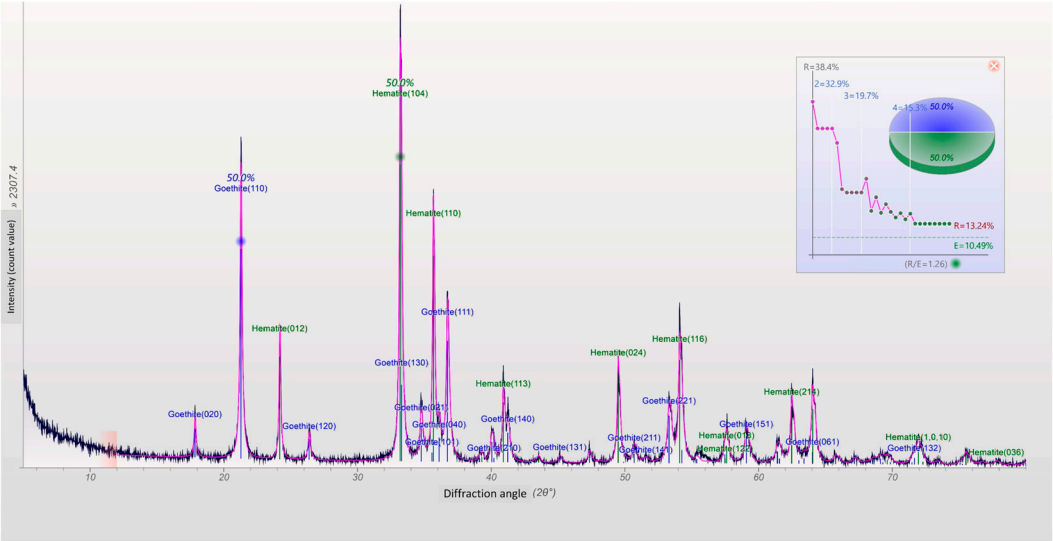

Figure 2. The XRD patterns of lump ore. R stands for Rwp (Weighted Profile R-factor), while 2, 3, and 4 represent the number of fitting iterations, essentially indicating the process of optimizing the R.

2.2. Experimental and Analysis Methods

The chemical composition of all samples was determined following the Chinese national standard method for iron ore analysis (GB/T 1361-2024 [31]).

Phase analysis was performed using a PANalytical X'Pert^3 Powder X-ray diffractometer (PANalytical Inc., Almelo, The Netherlands) with a Cu target X-ray tube. The operating parameters included a typical scanning range of 10–80°, a step size of 5°/min, and a tube power of 2.2 kW (voltage: 20–60 kV, current: 2–60 mA).

Simultaneous thermogravimetric and differential scanning calorimetry (TG-DSC) was conducted to identify physical and chemical transformations. Analyses were carried out in an air atmosphere using a STA449F3 instrument (NETZSCH, Selb, Germany), heating samples from room temperature to 1400 °C at a rate of 10 °C/min.

The thermal cracking index of the lump ore was determined according to the national standard GB/T 10322.6-2022 [32]. The procedure involved rapidly heating the sample to 700 °C within 30 min, maintaining this temperature for 30 min, cooling, and then sieving. The index is calculated from the mass percentage passing through a 6.3 mm sieve.

The softening and melting–dripping behavior was evaluated as per the Chinese standard GB/T 34211-2017 [33]. Tests were conducted under a reducing gas mixture (30% ± 0.5% CO, 70% ± 1% N_2) at a flow rate of 5.0 ± 0.1 L/min. A prepared sample in a graphite crucible was heated under load according to a programmed schedule until slag and metal dripping occurred. The sample compression and pressure drop were monitored in real time using an inductive displacement sensor and a differential pressure transducer, respectively. The furnace temperature, controllable up to 1650 °C, was measured with a Pt-Rh thermocouple. All data were recorded automatically.

- Softening start temperature (T_a): the temperature at which the sample's linear contraction reaches 10%, in °C.
- Softening end temperature (T_s): the temperature at which the sample's linear contraction reaches 40%, in °C.
- Dripping temperature (T_d): the temperature at which the sample's slag and iron begin to drip, in °C.
- Softening temperature range: $\Delta T_{sa} = (T_s - T_a)$, in °C.
- Soft-melting temperature range: $\Delta T_{ds} = (T_d - T_s)$, in °C.

The evaluation of softening–melting performance, based on the characteristic softening temperature and temperature range, provides insight into the position and thickness of the cohesive zone each material would form in a blast furnace. This analysis is critical for determining the material's effect on gas permeability within this zone.

3. Results and Discussion

3.1. Thermogravimetric Analysis

To investigate the thermal behavior of lump ore, thermogravimetric–differential scanning calorimetry (TG-DSC) was performed. The results for all three materials are presented in Figure 3.

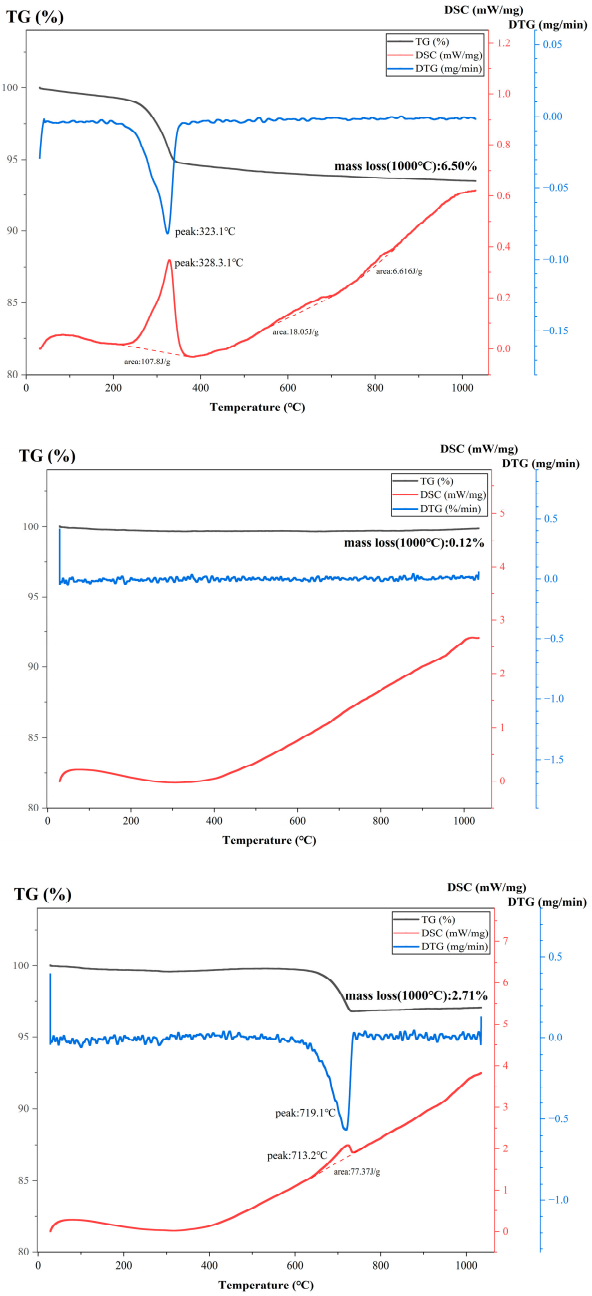

Figure 3. TG-DSC curves of the lump ore (PB) (**a**), TG-DSC curves of the pellets (**b**), and TG-DSC curves of the sinter (**c**).

As shown in Figure 3a, the lump ore exhibits distinct mass loss stages. An initial mass loss of approximately 1% below 200 °C is primarily attributed to the removal of adsorbed

water. A significant endothermic reaction occurs around 325 °C, within a rapid mass-loss phase between 220 °C and 380 °C. This corresponds to the decomposition and removal of crystalline water, accounting for a further ~5% mass loss. The curve stabilizes thereafter, with a final residual mass of 93.5%.

In contrast, the pellet (Figure 3b) demonstrates negligible mass loss below 1000 °C, indicating superior thermal stability. The sinter (Figure 3c) shows a minor mass loss of about 3% at 715–720 °C, associated with carbonate ($CaCO_3$) decomposition, with no discernible endothermic peak for crystalline water removal.

In summary, the lump ore undergoes significant mass loss due to dehydration, while the sinter exhibits loss from carbonate decomposition, and the pellet remains largely stable. Comparatively, the lump ore contains a moderate proportion of crystalline water.

3.2. Thermal Burst Performance of Lump Ore

The thermal burst index characterizes the fragmentation of lump ore upon heating in the upper blast furnace. A lower index indicates less fines generation in the solid charge zone, leading to improved permeability and more stable furnace operation. As shown in Table 4, the tested lump ore exhibits a relatively favorable thermal burst performance.

Table 4. Burst index of the lump ore.

Lump Ore	$DI_{-6.3}$ (%)	$DI_{-3.15}$ (%)	$DI_{-0.5}$ (%)
Burst index	13.9	7.4	0.8

- Burst index ($DI_{-6.3}$ $DI_{-3.15}$ $DI_{-0.5}$): Mass fraction of particles passing through a (6.3/3.15/0.5) mm sieve, %

3.3. Reduction Behaviors of the Furnace Burdens

Figure 4a presents the reduction performance of the different burden materials. The results indicate that the lump ore exhibits superior reducibility compared to the sinter, which in turn outperforms the pellet.

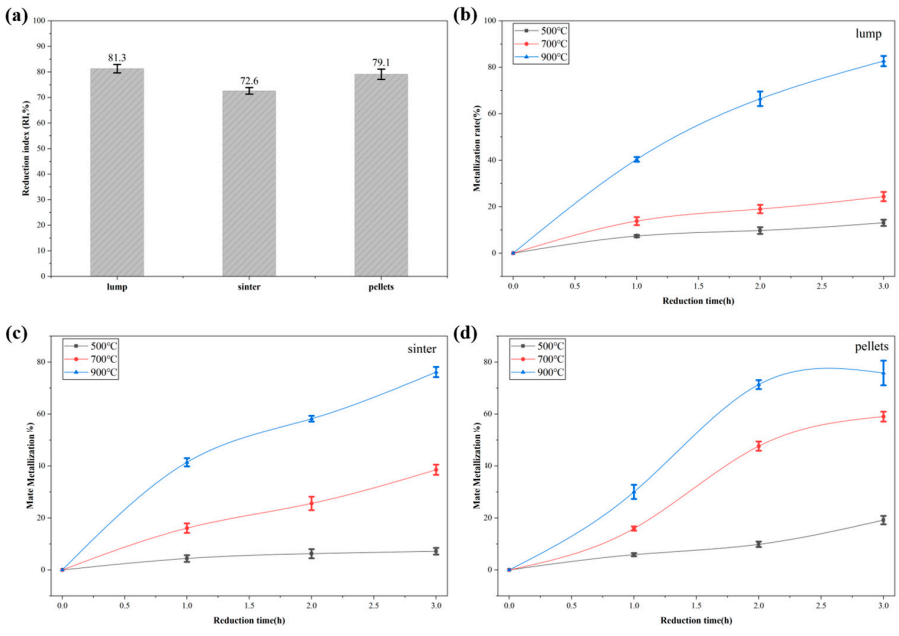

Figure 4. Reduction index (RI) of different blast furnace burdens (lump, pellets, sinter) (**a**), reduction behavior of lump ore at 500 °C, 700 °C, and 900 °C (**b**), reduction behavior of sinter at different temperatures (**c**), reduction behavior of pellets at different temperatures (**d**).

The reduction behavior across temperatures is shown in Figure 4b–d. For lump ore, the degree of metallization increases gradually at lower temperatures. This rate rises with increasing temperature and reduction time, showing a significant acceleration upon reaching 900 °C.

- Reduction index (RI): Mass fraction of metallic iron in the reduced sample relative to total iron, %.

3.4. Reduction Disintegration of Furnace Burdens

Table 5 presents the low-temperature reduction disintegration performance of the different burden materials. The results show that the pellet ore exhibits the best low-temperature reduction disintegration performance, followed by the lump ore, with the sinter demonstrating the comparatively inferior performance.

Table 5. The low-temperature reduction and pulverization properties of different blast furnace burdens.

Kind	Low-Temperature Reduction Disintegration Performance/%		
	$RDI_{+6.3\ mm}$	$RDI_{+3.15\ mm}$	$RDI_{-0.5\ mm}$
Lump ore	76.60	86.90	6.10
Pellets	97.70	97.90	2.10
Sinter	51.50	76.80	6.60

3.5. The Soft-Melting Properties of Burdens

The softening and melting–dripping properties of the single-ore burdens are summarized in Tables 6 and 7, respectively.

Table 6. The load softening properties of different blast furnace burdens.

Kind	Load Softening Properties/°C		
	T_{10}	T_{40}	$T_{40} - T_{10}$
Lump ore	922	1144	222
Pellets	1056	1135	79
Sinter	1170	1262	92

Table 7. The melting and dripping properties of different blast furnace burdens.

Kind	Melting and Dripping Properties/°C		
	T_s	T_d	$T_d - T_s$
Lump ore	1217	1366	149
Pellets	1162	1418	256
Sinter	1294	1535	241

As shown in Table 6, the lump ore is characterized by a relatively low initial softening temperature and a wide softening range. This combination is likely to result in a thickened cohesive zone within the blast furnace, adversely affecting gas permeability.

Conversely, the melting–dripping data in Table 7 reveals that the lump ore has a comparatively narrow cohesive range. In contrast, the cohesive ranges for both the pellet and the sinter exceed 240 °C.

Table 8 and Figure 5 present the softening performance of various burden structures with lump ore proportions ranging from 25% to 34%. The data reveal a clear positive correlation: as the proportion of lump ore (PB) increases, the initial softening temperature rises consistently.

Table 8. Impact of lump ore proportion (PB) on the softening temperature range of mixed burdens.

Blast Furnace Charge Structure	Load-Softening Performance/°C		
	T_{10}	T_{40}	$T_{40} - T_{10}$
Sinter 60% + Pellets 15% + Lump ore 25%	1076	1241	164
Sinter 60% + Pellets 12% + Lump ore 28%	1088	1247	159
Sinter 60% + Pellets 9% + Lump ore 31%	1090	1247	157
Sinter 60% + Pellets 6% + Lump ore 34%	1099	1255	156

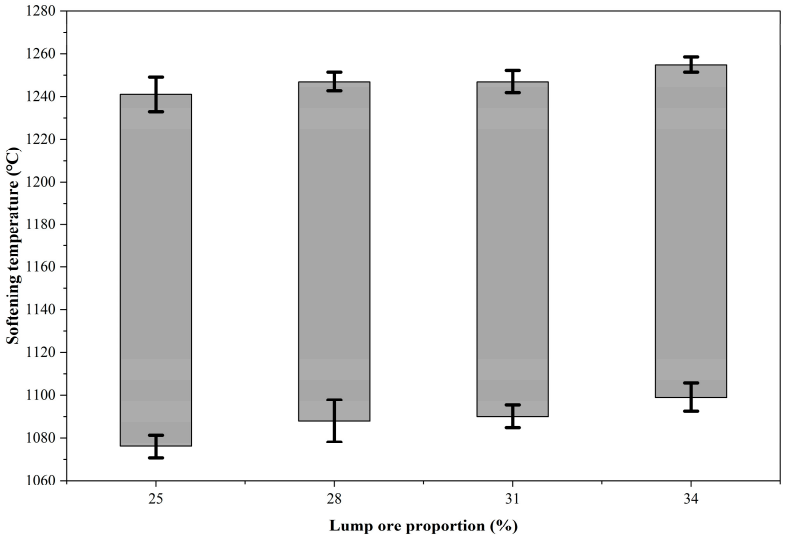

Figure 5. Impact of lump ore proportion (PB) on the softening temperature range of mixed burdens.

Specifically, at a lump ore proportion of 25%, the softening temperature is relatively low. This temperature increases progressively at proportions of 28% and 31%, reaching its highest level when the proportion attains 34%.

3.6. Melting and Dripping Performance of Various Burden Materials

Table 9 presents the melting and dripping performance under different charge structures, specifically examining the melting and dripping performance under various lump ore ratios (25–34%).

Table 9. Impact of lump ore proportion (PB) on the melting and dripping temperature range of mixed burdens.

Blast Furnace Charge Structure	Melting and Dripping Performance/°C			
	T_s	T_d	$T_d - T_s$	ΔP_{max} KP
Sinter 60% + Pellets 15% + Lump ore 25%	1304	1445	141	9.8
Sinter 60% + Pellets 12% + Lump ore 28%	1304	1473	169	3.3
Sinter 60% + Pellets 9% + Lump ore 31%	1301	1453	152	12.1
Sinter 60% + Pellets 6% + Lump ore 34%	1304	1460	156	12.1

Figure 6 illustrates the variation in the softening–melting zone characteristics of the burden structure across different lump ore ratios.

The analysis reveals three key trends. First, the initial softening temperature (T_s) remains stable between 1301 °C and 1304 °C, showing no significant change with increasing lump ore proportion. Second, the dripping temperature (T_d) exhibits a non-linear response: it initially rises from 1445 °C to 1473 °C as the ratio increases from 25% to 28%, then fluctuates slightly (1453 °C at 31%, 1460 °C at 34%). Consequently, third, the width of the

cohesive zone ($T_d - T_s$) first widens significantly from 141 °C to 169 °C, then narrows modestly but stabilizes at a higher level (152 °C at 31%, 156 °C at 34%).

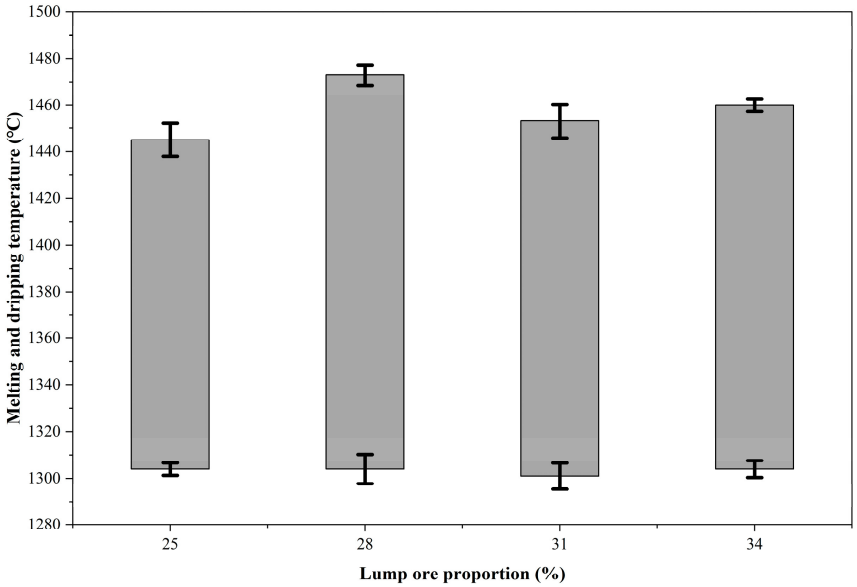

Figure 6. Impact of lump ore proportion (PB) on the melting and dripping temperature range of mixed burdens.

Figure 7 presents SEM images at varying magnifications of droplet samples collected from the softening and melting experiments. The microstructure consists predominantly of metal oxides and silicates, with minor metallic phases.

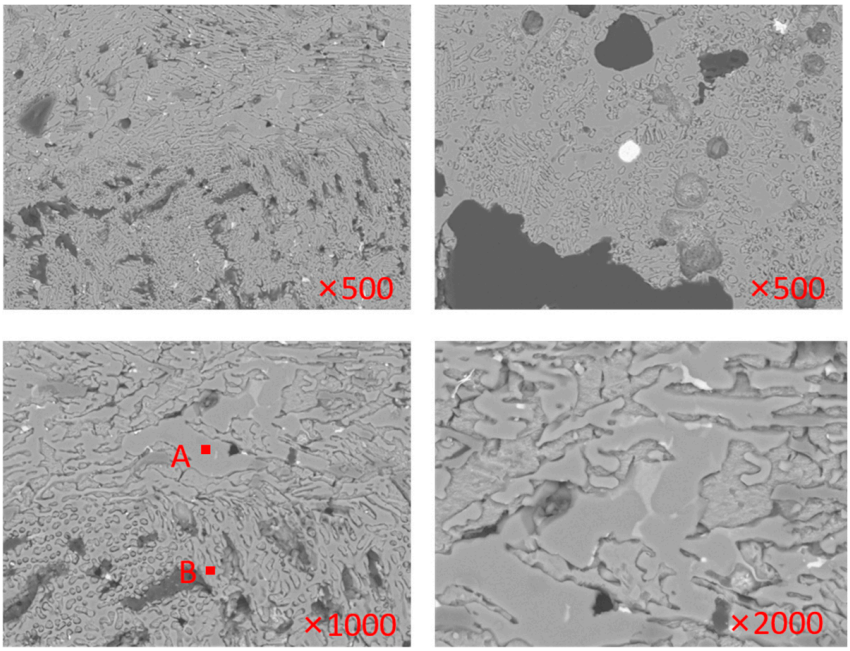

Figure 7. The SEM images of the samples dripped during the furnace charge melting and dripping experiment.

Energy-dispersive spectroscopy (EDS) was performed at points A and B (Figure 7), with the elemental compositions summarized in Table 10. Based on these compositions, the calculated starting melting temperatures are 1295.16 °C for point A and 1360.62 °C for point B.

Table 10. EDS analysis of the samples dripped during the furnace charge melting and dripping experiment.

Element (At, %)	A	B
O	50.12	49.07
Mg	4.21	12.09
Al	12.67	12.6
Si	14.5	10.75
Ca	18.49	15.49

The lower melting temperature at point A is consistent with the observed relatively low softening temperature of the lump ore. Furthermore, the presence of high-melting-point solid phases within the microstructure, as visible in the SEM images, suggests the formation of a comparatively wide cohesive (melting and dripping) zone.

3.7. Analysis Between Laboratory Properties and Industrial Practice

The correlation between key laboratory indices and actual blast furnace performance is summarized as follows: The laboratory lump ore showed a low thermal decrepitation index ($DI_{-6.3}$ = 13.9%). This corresponded to good permeability in the upper stack of the industrial furnace, with a stable pressure differential (ΔP) of 8–10 kPa and no issues related to fines accumulation. The high laboratory reduction index of the lump ore (RI = 81.3%), compared to sinter (72.6%), correlated with an increase in the industrial top gas utilization rate from 42% to 45%. This enhancement in indirect reduction contributed to a coke ratio reduction of 24 kg/t·Fe. The optimized mixed burden containing 28% lump ore exhibited a narrow laboratory softening interval of 159 °C—significantly less than that of single lump ore (222 °C). Industrially, this translated to a thinner cohesive zone, reduced gas flow resistance, and a stable furnace productivity (utilization coefficient). Based on these correlative results, a screening and proportioning standard for high lump ore burdens is proposed. This framework provides direct guidance for industrial application. The blast furnace fuel ratio is a core indicator for measuring the energy consumption and low-carbon performance of blast furnace ironmaking.

4. Industrial Production Practice

Based on the established slag system, the blast furnace burden structure was optimized. Guided by the laboratory findings and integrated with operational experience, industrial trials were subsequently conducted for smelting with a high proportion of lump ore.

Analysis of Industrial Production Practice Results

As shown in Figure 8c, the blast furnace burden was successfully optimized to sustain a high lump ore ratio. At the Ironmaking Plant, the monthly average lump ore proportion reached 28.37% in February 2023 and remained at or above this 28% benchmark. Performance improved further in the following months, with averages of 29.56% in March and 29.14% in April 2023. Notably, the lump ore ratio achieved or exceeded 30% on 16 days in March, while maintaining the overall monthly average above 28%.

Through this practice, the operational system for a high lump ore burden was refined, culminating in the establishment of an efficient, low-carbon smelting technical system for blast furnaces utilizing a high proportion of lump ore.

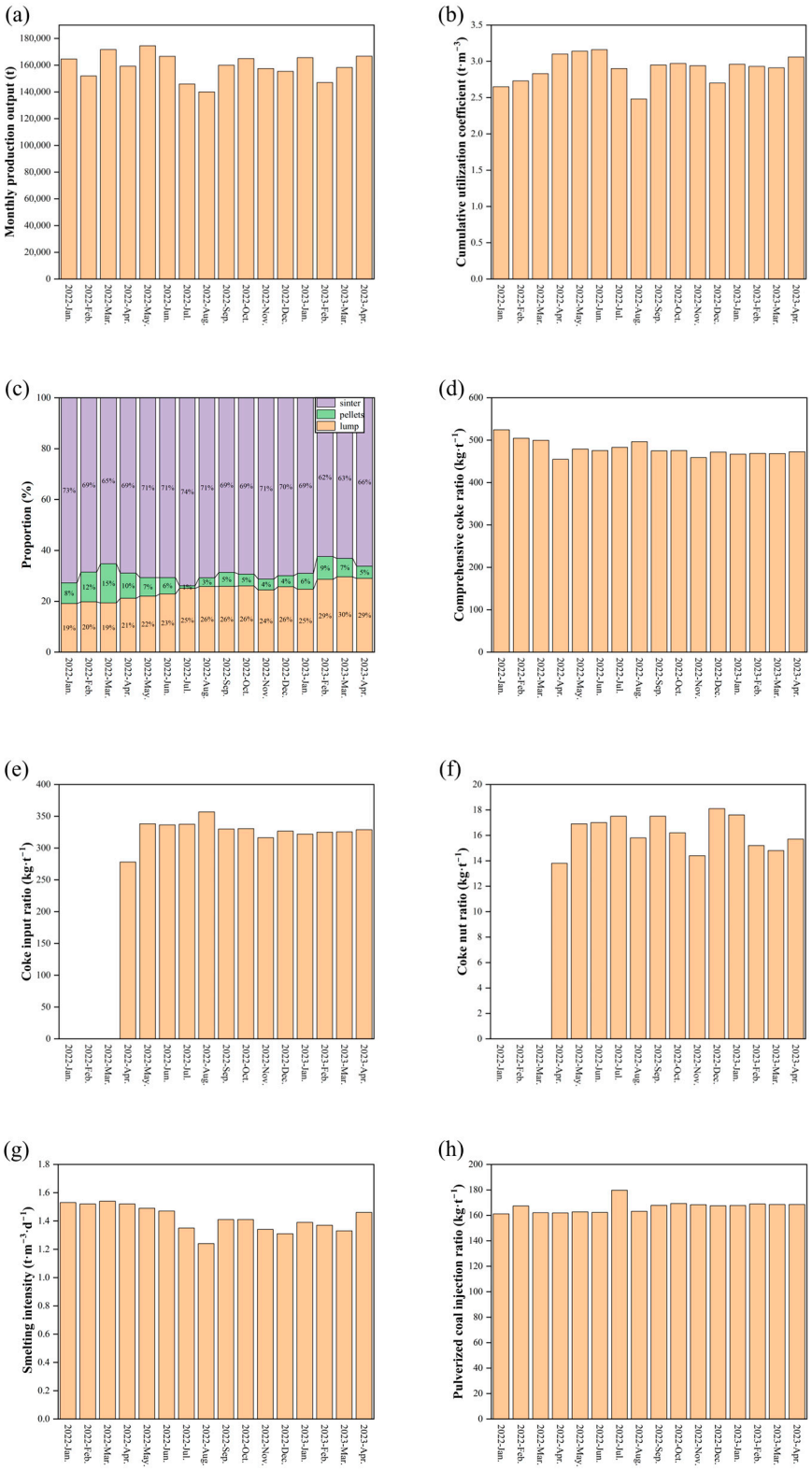

Figure 8. (**a**) Monthly output of the Ironmaking Plant (January 2022–April 2023); (**b**) Cumulative utilization coefficient of the Ironmaking Plant (January 2022–April 2023); (**c**) Monthly burden proportion of blast furnace in the Ironmaking Plant (January 2022–April 2023); (**d**) Monthly comprehensive coke ratio of the Ironmaking Plant (January 2022–April 2023); (**e**) Monthly coke input ratio of the Ironmaking Plant(April 2022–April 2023); (**f**) Monthly coke nut ratio of the Ironmaking Plant (April 2022–April 2023); (**g**) Monthly smelting intensity of the Ironmaking Plant (January 2022–April 2023); (**h**) Monthly Pulverized coal injection ratio of the Ironmaking Plant (January 2022–April 2023).

Figure 8f illustrates that as the lump ore proportion increased, the blast furnace utilization coefficient remained stable, while both the coke and slag ratios exhibited a declining trend.

Economically, from January 2022 to September 2023, the use of 1.8742 million tons of lump ore to replace pellets generated significant savings. With pellet and lump ore prices at 1116.5 and 959.5 CNY/ton, respectively, this substitution reduced molten iron production costs by CNY 294.3 million.

In terms of carbon emissions, the operational optimization culminated in a record-low fuel ratio of 505.93 kg/t·Fe across five blast furnaces in January 2023. Furthermore, replacing pellets with lump ore avoided considerable energy consumption, specifically 11,159.2 MWh of electricity and 608,111.0 GJ of gas.

The strong correlation between laboratory properties and industrial performance is evidenced in two key areas: The lump ore's superior laboratory reduction index (RI = 81.3% vs. sinter's 72.6%) and its higher metallization rate at 900 °C corresponded directly to enhanced industrial performance. This manifested as an increase in the top gas utilization rate from 42% to 45%, improved indirect reduction, and a consequent reduction in the coke ratio. The lump ore's favorable physical properties—a low thermal decrepitation index ($DI_{-6.3}$ = 13.9%) and better low-temperature reduction disintegration ($RDI_{-0.5}$ = 6.1%) compared to sinter—were reflected in stable and efficient furnace operation. Industrially, this translated to a stable permeability, with a pressure differential (ΔP) maintained between 8 and 10 kPa, free from issues like channeling or hanging.

The successful industrial increase in lump ore proportion from 25% to monthly averages of 28.37% (February), 29.56% (March), and 29.14% (April) 2023 resulted in stable and efficient operation. The blast furnace utilization coefficient remained stable at approximately 2.85 t/(m^3·d), while the coke ratio decreased by 4.2% (from 528 to 505.93 kg/t·Fe) and the slag ratio decreased by 4.7% (from 320 to 305 kg/t·Fe). Critically, the high lump ore proportion (≥28%) did not destabilize the furnace. This is attributed to the laboratory-optimized mixed burden, which achieved a narrow softening–melting interval of 159 °C (Table 8). This optimization effectively mitigated the inherent drawback of a wide softening interval observed in single lump ore (222 °C), ensuring a moderate cohesive zone thickness and maintaining good overall permeability.

5. Conclusions

Lump ore represents a zero-carbon-emission blast furnace burden. Therefore, partially substituting sinter and pellets with lump ore to optimize the burden structure is a significant pathway for iron and steel plants to reduce carbon emissions. This study systematically investigated the evolution of lump ore in the solid-state zone, its softening and dripping behavior in the cohesive zone, and the optimization of the overall burden structure under high-lump-ore conditions. The aim was to develop new technologies for low-carbon, high-efficiency smelting.

Analysis of the lump ore's physicochemical properties revealed it had the highest total iron content, a primary size fraction of 16–25 mm, and a mineralogy dominated by hematite (Fe_2O_3) and goethite (FeO(OH)). In terms of performance, the lump ore demonstrated superior reducibility compared to sinter, which in turn outperformed pellets. However, regarding low-temperature degradation, pellets exhibited the best stability while sinter performed the worst. A key challenge identified was that lump ore's lower initial softening temperature and wider softening range could, if not managed, broaden the overall burden's softening interval. This risked thickening the blast furnace's cohesive zone and impairing permeability.

Production practice confirmed that these challenges can be overcome. By strategically selecting lump ore based on its metallurgical properties and decrepitation index, and by carefully proportioning it within the burden while adjusting the sinter's properties for complementarity, a charge with excellent overall metallurgical performance can be achieved. Through corresponding adjustments to the blast furnace operational system, a comprehensive lump ore proportion of $\geq$28% was successfully implemented. This optimization resulted in a reduced fuel ratio of $\leq$515 kg/t·Fe, demonstrating the viability of high-lump-ore operation for low-carbon ironmaking. Scaling this improvement to an annual hot metal production of 1 million tons translates to fuel savings of 15,000–35,000 tons per year. Based on a fuel carbon content of 0.85, this equates to an annual CO_2 emission reduction of approximately 45,000–105,000 tons, a performance metric that significantly surpasses the industry average.

Author Contributions: Conceptualization, Y.G. and S.W.; methodology, Y.X., F.C., and S.W.; validation, Y.X. and F.C.; formal analysis, L.Y. and L.F.; investigation, Y.X. and H.J.; resources, L.F. and H.J.; data curation, S.W., L.Y. and H.J.; writing—original draft preparation, S.W., Y.X. and H.J.; writing—review and editing, Y.G., L.F., and F.C.; supervision, Y.G. and S.W.; project administration, S.W. and L.F.; funding acquisition, Y.G. All authors have read and agreed to the published version of the manuscript.

Funding: This research received no external funding.

Data Availability Statement: The original contributions presented in this study are included in the article. Further inquiries can be directed to the corresponding author.

Conflicts of Interest: Authors Lei Fang and Heming Ju were employed by the company Nanjing Steel Group Co., Ltd. The remaining authors declare that the research was conducted in the absence of any commercial or financial relationships that could be construed as a potential conflict of interest.

References

1. Peacey, J.G.; Davenport, W.G. *The Iron Blast Furnace: Theory and Practice*; Elsevier: Amsterdam, The Netherlands, 2016.
2. Guo, Y.; Zhang, Y.; Chen, F.; Wang, S.; Yang, L.; Xie, Y.; Xia, X. Optimizing high-Al_2O_3 limonite pellet performance: The critical role of basicity in consolidation and reduction. *Metals* **2025**, *15*, 801. [CrossRef]
3. Pan, Y.; Zuo, H.; Wang, J.; Xue, Q.; Wang, G.; She, X. Review on improving gas permeability of blast furnace. *J. Iron Steel Res. Int.* **2020**, *27*, 121–131. [CrossRef]
4. Loo, C.E.; Matthews, L.T.; O'dea, D.P. Lump ore and sinter behaviour during softening and melting. *ISIJ Int.* **2011**, *51*, 930–938. [CrossRef]
5. Wang, Y.-Z.; Zhang, J.-L.; Liu, Z.-J.; Du, C.-B. Recent advances and research status in energy conservation of iron ore sintering in China. *Jom* **2017**, *69*, 2404–2411. [CrossRef]
6. Fernández-González, D.; Ruiz-Bustinza, Í.; Mochón, J.; González-Gasca, C.; Verdeja, L.F. Iron ore sintering: Process. *Miner. Process. Extr. Metall. Rev.* **2017**, *38*, 215–227. [CrossRef]
7. Li, Z.; Fan, X.; Yang, G.; Wei, J.; Sun, Y.; Wang, M. Life cycle assessment of iron ore sintering process. *J. Iron Steel Res. Int.* **2015**, *22*, 473–477. [CrossRef]
8. Zhu, D.; Jiang, Y.; Pan, J.; Yang, C. Study of mineralogy and metallurgical properties of lump ores. *Metals* **2022**, *12*, 1805. [CrossRef]
9. Wu, S.-L.; Xu, H.-F.; Tian, Y.-Q. Evaluation of lump ores for use in modern blast furnaces as part of mixed burden practice. *Ironmak. Steelmak.* **2009**, *36*, 19–23. [CrossRef]
10. Wu, S.; Han, H.; Xu, H.; Wang, H.; Liu, X. Increasing lump ores proportion in blast furnace based on the high-temperature interactivity of iron bearing materials. *ISIJ Int.* **2010**, *50*, 686–694. [CrossRef]
11. Liu, L.G.; Chen, L.S. The practice of improving ratio of lump ore for BF#6 at SGIS. *South. Met.* **2019**, *5*, 37–39+49.
12. Ma, Y.; Tang, L.; Zhang, Y. Experimental research and applization of the utilization ratio of lump ore in blast furrnace of Anyang Steel. *Henan Metall.* **2020**, *28*, 4–5+42.
13. Sun, B.; Zhou, X.; An, Y.; Yu, X. Analysis of metallurgical properties of Qingdao special steel blast furnace block ore. *Shandong Metall.* **2020**, *42*, 45–47.

14. Li, Y.F.; He, Z.J.; Zhan, W.L.; Kong, W.G.; Han, P.; Zhang, J.H.; Pang, Q.H. Relationship and mechanism analysis of soft-melt dropping properties and primary-slag formation behaviors of the mixed burden in increasing lump ore ratio. *Metals* **2020**, *10*, 1254. [CrossRef]
15. Zhang, H.; Tang, J.; Zhou, M.S.; Xia, T.Y.; Liu, J.; Zhai, L.W.; Xu, L.B. Study on types and proportion of lump ore charged into blast furnace in Ansteel. *Angang Technol.* **2022**, 15–19+30.
16. Kong, Y.D.; Chen, Y.C.; Hu, L.C. Industrial test of higher lump ore percentage in Zhongtian Steel No.3 BF. *Ironmaking* **2024**, *43*, 25–30.
17. Li, W.; Tang, Y.; Ma, X. Production practice of increasing the consumption of steel blast furnace. *Shanxi Metall.* **2024**, *47*, 151–154.
18. Wang, Y.; Xia, W. Measures to increase lump ore ratio in Handan Steel No. 1 blast furnace. *Ironmaking* **2024**, *43*, 19–23.
19. Wang, Q.; Wang, J.; Zhang, X.; Fen, Z. Process trial of crushing, screening, and dry pre-selection for a certain iron ore. *Mod. Min.* **2024**, *40*, 139–144.
20. Faria, G.L.; Tenório, J.A.S.; Jannotti, N.; Araújo, F.G.d.S. Disintegration on heating of a Brazilian manganese lump ore. *Int. J. Miner. Process.* **2013**, *124*, 132–137. [CrossRef]
21. Zhao, Q.; Xiao, H.; Wei, J.; Yi, L.; Ma, Z.; Zhang, N.; Hu, C. Study on the physicochemical properties and thermal cracking behavior of typical PB lump ore. *Sinter. Pelletizing* **2021**, *46*, 72–77.
22. Zhao, H.; Sun, Y.; Wang, Y.; Gao, L.; Zhang, F.; He, Z.; Zhang, J. Influencing factors and reaction mechanism of thermal bursting of blast furnace lump ore. *Energy Metall. Ind.* **2025**, *44*, 26–32.
23. Yi, L.; Hao, H.; Shen, X.; Shu, Y.; Xiao, H.; Zhong, Q.; Zhang, X. Thermal decrepitation of Pilbara (PB) lump ore: Characteristic, mechanism, and inhibitory strategy. *Powder Technol.* **2023**, *430*, 119016. [CrossRef]
24. Song, S.; Zhao, Z. High lump iron ore proportion production practice of Hanbao Iron. *Gansu Metall.* **2021**, *43*, 11–13.
25. Zhang, H.; Chen, L.; Shi, Z. Production practice of high-block ore in Xingcheng blast furnace compared to smelting. In Proceedings of the 14th China Iron and Steel Annual Conference, Chongqing, China, 25–26 October 2023; p. 6.
26. Li, Y.; Xie, S.; Liu, X.; Wang, D.; She, X. Research on measures to increase the proportion of lump ore in blast furnace. *Shanxi Metall.* **2024**, *47*, 177–180.
27. Zeng, Z.; She, X.; Guo, Z.; Chen, W.; Li, Q.; Wang, J.; Wang, D. Optimization of the proportion of lump ores based on the basic properties and interaction reactions of iron-bearing materials. *ISIJ Int.* **2025**, *65*, 1803–1811. [CrossRef]
28. Heikkilä, A.; Iljana, M.; Bartusch, H.; Fabritius, T. Reduction of iron ore pellets, sinter, and lump ore under simulated blast furnace conditions. *Steel Res. Int.* **2020**, *91*, 2000047. [CrossRef]
29. Lu, L.; Holmes, R.; Manuel, J.; Edenton, A.; Adam, M.; Smyth, R.; Hapugoda, S. Lump ore characteristics and their impact on blast furnace operation. In Proceedings of the Iron Ore Conference, Perth, WA, Australia, 27–29 July 2009.
30. Zhang, J.; Hao, L.; Liu, Z.; Feng, B.; Niu, L.; Li, S.; Li, Z.; Wang, Y. The Temperature of Pretreatment on Microstructure Change of Lump Ore and Improvement of Metallurgical Properties. *Steel Res. Int.* **2024**, *95*, 2400074. [CrossRef]
31. *GB/T 1361-2024*; General Rules and Regulations for Analysis of Iron Ores. Standards Press of China: Beijing, China, 2024.
32. *GB/T 10322.6-2022*; Iron Ores for Blast Furnace Feedstocks—Determination of the Decrepitation Index. Standards Press of China: Beijing, China, 2022.
33. *GB/T 34211-2017*; Iron Ores—Method for Determination of Iron Reduction Softening Drippinger Performance Under Load. Standards Press of China: Beijing, China, 2017.

Disclaimer/Publisher's Note: The statements, opinions and data contained in all publications are solely those of the individual author(s) and contributor(s) and not of MDPI and/or the editor(s). MDPI and/or the editor(s) disclaim responsibility for any injury to people or property resulting from any ideas, methods, instructions or products referred to in the content.